J Solid State Electrochem (2004) 8: 763–771
DOI 10.1007/s10008-004-0543-8

ORIGINAL PAPER

Katarzyna Slowinska · Marcin Majda

Measurements of the capacitance and the response time of solid-state potentiometric sensors by an electrochemical time-of-flight method

Received: 3 April 2004 / Accepted: 24 April 2004 / Published online: 14 August 2004

Abstract A micro-electrochemical time-of-flight technique relying on galvanostatic ion generation and potentiometric sensing (P-ETOF) has been developed in order to characterize dynamic properties of solid-state potentiometric sensors and to measure their capacitance. Lithographically-fabricated generator-sensor devices featuring 10 μm-wide micro-electrodes spaced by 20–50 μm are used in either an open face mode, where hemicylindrical diffusion governs mass transport of generated ions, or in a narrow channel mode, where linear diffusion describes transport of ions between the generator and sensor micro-electrodes in a thin (~3 μm) layer of electrolyte. P-ETOF-open face mode is capable of generating silver ions or protons at a rate equivalent to a current density of 10 A/cm^2. This induces a maximum, mass transport controlled rate of a sensor potential rise of ~80 V/s. P-ETOF was used to characterize anodically electrodeposited iridium oxide film pH micro-sensors. Their maximum rate of potential change was determined to depend inversely on the oxide film's thickness and varied from 34 V/s for 40 nm-thick films to 9 V/s for the 650 nm-thick iridium oxide films. The capacitances of these pH micro-sensors were determined to depend linearly on their thicknesses, with a slope of 3 μF cm^{-2} nm^{-1} and a specific capacitance of 30 F/cm^3. These results point to slow proton transport in the bulk of the oxide film as a mechanistic element of their pH response.

Keywords Band microelectrode · Solid-state micro-potentiometric sensors

Dedicated to Zbigniew Galus on the occasion of his 70th birthday.

K. Slowinska · M. Majda (✉)
Department of Chemistry, University of California,
Berkeley, CA 94720–1460, USA
E-mail: majda@berkeley.edu
Fax: +1-510-6420269

Introduction

Micro-potentiometric sensors have found an increasing range of applications in medicine, biological sciences, industrial process monitoring, and analytical measurements and techniques such as scanning electrochemical microscopy [1, 2, 3, 4, 5, 6, 7, 8]. These new uses of miniaturized potentiometric sensors call for characterization of their response time and capacitance in addition to the usually-examined selectivity and sensitivity. These parameters could be crucial or limiting to their performance. Also, due to some nuances of their microfabrication procedures, these parameters could simply be different to those obtained for similar, macroscopic sensors. In this report we present a novel methodology allowing us to measure both the response time (the highest rate of electrode potential change) and capacitance of solid-state micro-potentiometric sensors.

The approach presented here involves a dual microelectrode electrochemical time-of-flight technique (ETOF) that relies on galvanostatic generation and potentiometric sensing [8]. As described recently, this technique is similar to the original amperometric ETOF technique introduced by Feldman et al [9] and used by others to measure diffusion constants of redox species [10, 11, 12, 13, 14]. Unlike amperometric ETOF, in which both the generator and collector micro-electrodes are operated under controlled potential conditions, in our method the generator micro-electrode is operated under constant current conditions, allowing us to control the rate of electro-generation of selected species [8]. Moreover, we rely on potentiometric sensing as a means of monitoring diffusion rates of the electro-generated species across the inter-electrode gap. In view of this, we refer to our technique as potentiometric ETOF (P-ETOF).

The general strategy in using P-ETOF to characterize response time of potentiometric sensors is straightforward. Application of large current steps to the generator micro-electrode, and positioning a micro-potentiometric sensor in close proximity to the generator ensure that

large fluxes of selected ions are created at the sensor microelectrode. This then necessitates its rapid response, challenging its rise-time capabilities. By analyzing the observed and the theoretically-expected sensor potential versus time (*E-t*) transients, we can determine the maximum rate of sensor potential change. Theoretical predictions can be obtained on the basis of either numerical simulations of ion diffusion, or analytical solutions of Fick's laws of diffusion in combination with the experimentally-determined Nernstian slopes of micro-sensors. This approach is somewhat different to the numerous literature methods that rely on generation of an "activity step", a rapid change of activity of species to which a potentiometric sensor exhibits selective response accomplished by forced convection [15, 16, 17, 18, 19, 20]. While a detailed review of those techniques is beyond the scope of this report, we point out that the method presented below is capable of measuring response times as high as ~80–100 V/s. This is similar to the capabilities of the sophisticated switched wall-jet method of Pungor et al, but does not require elaborate instrumentation [21]. Admittedly, by design, our approach does not offer the capability of a square concentration pulse that the "activity step" techniques strive to achieve. Therefore, *E-t* transients obtained in P-ETOF experiments are not directly comparable to those obtained by the activity step methods. Nevertheless, the maximum rate of potential change obtained in the P-ETOF experiment is a parameter that meaningfully reflects the sensor's response kinetics.

In order to test the capabilities of our P-ETOF technique, we first investigate the time response of a simple silver micro-potentiometric sensor. The Ag^+/Ag system was selected because of its very rapid electron transfer kinetics characterized by k_0 of 0.25 cm/s [22]. Subsequently, P-ETOF is used to assess the time response of anodically electro-deposited iridium oxide films (AEIROF) that are known to act as well-behaved pH micro-sensors [5, 6, 20, 23, 24, 25, 26, 27, 28, 29, 30].

Capacitance of potentiometric sensors is a parameter rarely of interest to practitioners of analytical potentiometry. However, as potentiometric sensors become miniaturized and find applications involving exceedingly small volumes of analyte solutions, such as those in medical and biophysiological areas and in SECM, the capacitance of a sensor becomes a parameter that could limit the accuracy of potentiometric measurements [4, 7]. We expand on this point below as we use P-ETOF to measure the capacitance of both the silver and AEIROF micro-sensors.

Experimental

Reagents

House-distilled water was passed through a three-cartridge Millipore purification train consisting of a Macropure pretreatment, an Organics Free cartridge for removal of trace organic contaminants, an ion-exchanger, and a 0.2 μm hollow-fiber final filter for removing particles. The resistivity of the resulting water (DI water) was ≈18.3 MΩ cm. A silver cyanide plating solution was purchased from Transene Co. and used as directed. Potassium tetrachloropalladate (99.99%, Alfa Aesar), iridium(IV) chloride (99.95%, Alfa Aesar), oxalic acid dihydrate (99%, Aldrich), hydrogen peroxide (30%, EM Science), lithium perchlorate (99.99%, Aldrich), sodium nitrate (ACS certified, Fischer Scientific), sulfuric acid (reagent grade, EM Science), and 3-mercaptopropyltrimethoxysilane (MPS, 95%, Aldrich) were all also used as received.

Fabrication and characterization of the generator-sensor micro-band devices

Two types of devices were used in this research. The P-ETOF experiments carried out in the "open-face" mode were done with a lithographically-fabricated gold dual-band micro-electrode device described previously [8]. The design of these devices features two, parallel, independently addressable, 10 μm-wide micro-band electrodes separated by a gap of 20 μm. One of the micro-bands functioned as a generator, the working electrode, and the other as a potentiometric sensor. A Pt counter electrode and an SCE reference electrode of a standard three-electrode galvanostatic circuit were immersed in the electrolyte solution and positioned directly in front of the dual micro-band device.

In the P-ETOF experiments carried out in a "narrow channel" mode used to measure the capacitance of the micro-sensors, we relied on the lithographically-fabricated (lift-off technology) gold-on-glass devices shown schematically in Fig. 1. In view of the expected high resistance of a thin layer solution trapped in a device, the generator micro-electrode is placed symmetrically with the two micro-sensors and the two counter electrode segments (shorted externally). The pseudo-reference electrode is silver-coated. Its potential in a 1 M $LiClO_4$ electrolyte did not drift in excess of ~2 mV in 10 s. The central area of the device is covered with a glass slide (marked by a dashed line in Fig. 1) and serves to create a narrow (2–3 μm-thick) channel confining electrolyte solution. The exact thickness of the channel is established by four polymer film spacers lithographically deposited in the corners of the cover slide, and achieved by a mechanical squeezing device. The role of this device is to limit the gap between the two glass slides to the exact thickness of the four spacers. The latter was confirmed in a set of standard thin-layer cell voltammetric experiments involving a standard $Ru(NH_3)_6^{3+}$ solution of known concentration reported elsewhere [31]. The lengths of all of the electrodes are defined by a thin, insulating polymer film (shown as the dotted area in Fig. 1). A more detailed description of the device fabrication protocol and the related post-fabrication procedures is available elsewhere [31].

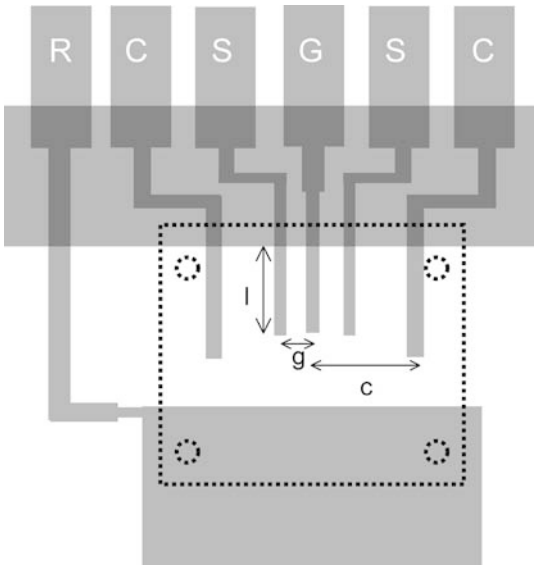

Fig. 1 A schematic drawing of a micro-electrode device used in P-ETOF (narrow channel mode) experiments showing the configuration of the micro-electrodes: generator (G), two symmetrically located sensors (S), two externally shorted counter electrodes (C), and a reference electrode (R). The width of the generator and the sensor micro-electrodes is 10 μm, their center-to-center separation (g) is 50 μm, and their length is ~1.5 mm. The latter is adjusted using the insulating polymer film, shown as a shaded rectangle. The dotted-line rectangle shows the position of a cover glass slide used to create a narrow channel above the micro-electrodes. The thickness (~3.0 μm) of the solution layer trapped between the glass slides is controlled by the thickness of the four polymeric spacer dots at the corners of the cover slide

Following their fabrication, the devices were chemically modified to suit their specific purpose. In the case of the Ag^+ P-ETOF experiments, both generator and sensor micro-band electrodes were electroplated with silver using a commercial silver-plating solution. This involved ~1 min galvanostatic electrolysis with 5 mA/cm^2 current density and resulted in ~0.7 μm-thick silver films. These were measured with a stylus profilometer (Alfastep 100 by Tencor, Inc). Much thinner Ag films (~10 nm) were formed on the sensor micro-electrodes. The Ag^+ P-ETOF experiments were done with non-deaerated electrolyte solutions. Modification of the devices used in the proton P-ETOF experiments involved electrochemically-induced precipitation of iridium(IV) oxide on the sensor micro-electrode [6, 33]. The process was initiated by a constant current (1 mA/cm^2) electro-reduction of an oxalate ligand of an iridium oxalate complex. The IrO_2 films obtained in this way were 20–120 nm in thickness depending on the duration of the electro-reduction. The generator micro-electrode did not require any modification steps. H^+ ions were generated by constant current electro-oxidation of water. We note that, while the concentration of oxygen exceeded its solubility in water near the generator micro-electrodes in the experiments carried out at high current densities, we did not observe nucleation of gaseous oxygen. This is fortunate in that severe disruption of proton diffusion between generator and sensor would otherwise result in high generator current experiments. Both the Ag and AEIROF sensor electrodes were calibrated by measuring their open circuit potential during a series of standard additions of $AgNO_3$ or sulfuric acid to a calibration solution. Following these modifications, the width of every generator and sensor electrode was measured microscopically (Reichert microscope) with a 0.2 μm precision. Electrode widths are used as input parameters in the digital simulations and in the analysis of the *E-t* transients as described below. Prior to all P-ETOF experiments, the initial pH was adjusted with $HClO_4$ if needed. To achieve low initial Ag^+ electrolytes, a $AgClO_4$ solution of a desired concentration was prepared and its actual concentration was measured potentiometrically (using a standard calibration curve) directly in the electrochemical cell immediately prior to P-ETOF experiments with a silver indicator electrode. The electrochemical measurements designed to obtain diffusion constants of the silver and hydrogen ions were described previously [8]. All electrochemical and ETOF experiments were carried out at 22 ± 0.5 °C.

Computations and computer simulations

Theoretical predictions of the *E-t* curves obtained in the open-face mode P-ETOF experiments were obtained by computer simulations executed using implicit finite difference simulations with a hemi-cylindrical geometry as described earlier [8, 33]. The theoretical *E-t* transients corresponding to those obtained in the P-ETOF–narrow channel mode experiments were computed using analytical solutions of the diffusion equations and a Matlab software package (v6.1.0.450, The MathWorks Inc). The sensor-potential transients were shown to follow the Nernst equation. The values of the Nernstian slopes were determined experimentally.

Instrumentation

All electrochemical measurements were performed with a CH Instruments Model 660A electrochemical analyzer. The instrument was customized by adding a potentiometry adapter to measure the potential difference between the sensor and a common reference electrode in addition (during chronopotentiometric experiments) to the measurements of the potential of the working electrode. This is possible through simultaneous two channel recording. The maximum sampling rate of each channel of this instrument is 2.5 ms. The resolution of the potential measurements is better then 0.5 mV.

Results and discussion

Measurements of sensor response time

In order to generate high fluxes of the Ag^+ or H^+ ions at the micro-sensor electrodes, we relied on the open face

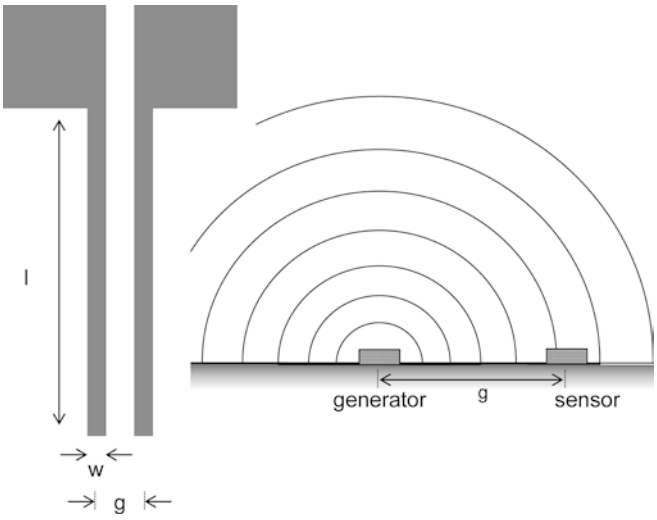

Fig. 2 Schematic drawings (top and cross-sectional views) of the generator-sensor device used in P-ETOF (open face mode) experiments. The width (w) and the length (l) of the micro-band electrodes are 10 μm and 2 mm, respectively. The inter-electrode gap (g) is 20 μm. The cross-sectional drawing illustrates the hemi-cylindrical diffusion of electro-generated species away from the generator micro-electrode

dual-band micro-electrode devices described in our previous report. A schematic diagram and the typical dimensions of the relevant parameters of such devices are shown in Fig. 2. The term "open face" (OF) refers to the fact that the P-ETOF experiments were carried out in an electrolyte solution of quasi-unrestricted volume allowing hemi-cylindrical propagation of the diffusion front of the electro-generated ions (see inset in Fig. 2). Under such conditions, the maximum applied generator current was 1.0×10^{-3} A, yielding a generator micro-electrode current density of approximately 10 A/cm^2. These values are limited by the structural stability of the lithographically-fabricated gold micro-electrodes. In order to elicit a large change in micro-sensor potential in response to a particular flux of the electro-generated ions, their initial concentration was selected to be low. Specifically, $[Ag^+]_{init}$ was in the range of 10^{-8}–10^{-7} M, and $[H^+]_{init}\approx1\times10^{-7}$ M. The slopes of the Nernstian response of the two micro-sensors in question were measured to be: Ag, 60 ± 1 mV/decade, AEIROF, 80 ± 2 mV/decade.

A set of E-t transients obtained in the Ag^+ P-ETOF experiments designed to measure the maximum rate of the potential change of the Ag micro-sensor are shown in Fig. 3. All of the experiments were carried out with high values of the generator current, including 1.0×10^{-3} A – the highest value reproducibly tolerated by our ETOF devices. As expected, the recorded E-t transients exhibit progressively increasing slope values ranging from ~15–85 V/s. Before we discuss these values, we want to address the significant discrepancies between the observed and the simulated E-t transients.

Transients A and B recorded for the highest generator currents are affected by migration in spite of high electrolyte concentration. These two E-t transients show, initially, higher plateau values than theoretically predicted. This phenomenon was discussed previously [8]. All of the experimental transients in Fig. 3 exhibit a positive shift, or a time delay that becomes progressively larger as the generator current decreases. This delay is due to the finite capacitance of the silver micro-sensor, a phenomenon described in detail in our previous report [8]. Briefly, a differential increase of the micro-sensor potential (dE, related to the charging of the sensor/solution interface) in a P-ETOF experiment in response to an increase in the activity of the Ag^+ ions requires electro-reduction of a certain quantity of silver ions (dN). The latter is proportional to the sensor's capacitance C_{dl}:

$$dN = \frac{C_{dl}(E)AdE}{nF} \tag{1}$$

This open circuit, double-layer charging results in a decrease of the Ag^+ ion concentration in the vicinity of the sensor relative to theoretical expectations, and causes

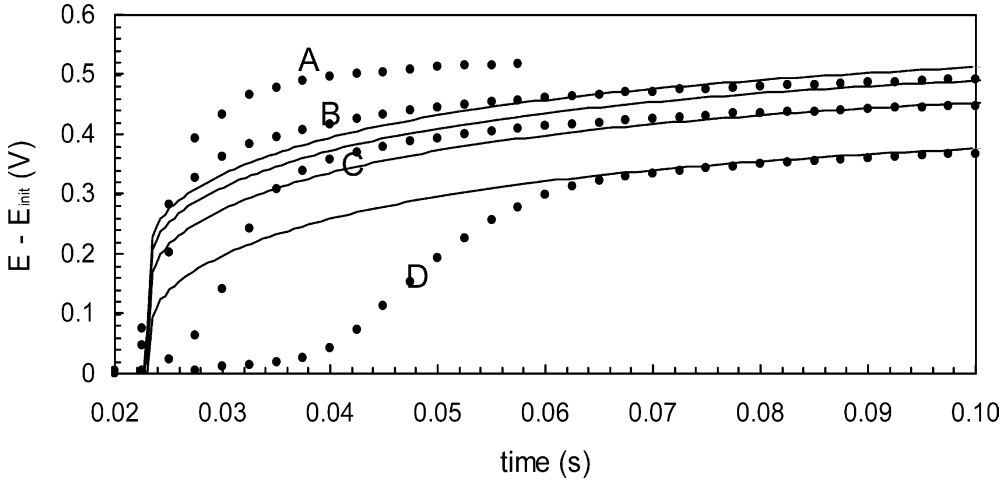

Fig. 3 A set of the experimental (dots) and simulated (lines) Ag^+ P-ETOF(OF) sensor potential versus time transients recorded with the 20 μm gap device of Fig. 2 in 1.0×10^{-8} M $AgNO_3$, 1 M $LiClO_4$ solution at a generator current of 1.0 mA (**A**), 0.5 mA (**B**), 0.1 mA (**C**), 0.01 mA (**D**). The simulations were obtained with a Ag^+ diffusion coefficient of 1.24×10^{-5} cm^2/s

delays in the onset of the potential rise, as seen in Fig. 3. Our theoretical *E-t* transients obtained by numerical simulations take into account solely the diffusion of silver ions and are based on an explicit assumption that the sensor is infinitesimally small and so $C_{dl}A = 0$. As we discussed earlier, a delay in sensor response is expected whenever the rate of increase of the sensor potential is high and the flux of the silver ions is low or, in other words, in cases of low supply and high demand [8]. Supply refers here to the instantaneous flux of Ag^+ ions at the sensor. It is proportional to the rate of generation (i_{gen}) of the silver ions, and inversely proportional to the inter-electrode gap. Demand, in this analogy, refers to the number of moles of silver ions, dN, that must be reduced to increase the sensor potential of a given surface area by a certain value, as shown by Eq. 1. It is proportional to the magnitude of the expected potential change, a quantity related to the initial silver ion concentration. Clearly, by adjusting $[Ag^+]_{init} = 1.0\times10^{-8}$ M we purposefully created "high demand" conditions in order to elicit a high rate of the sensor potential change at the expense of generating substantial capacitive delays [8].

Returning now to the data in Fig. 3, we must first understand what process limits the maximum slope of the *E-t* transients: electron transfer or silver ion mass transport. The theoretically-expected rate of silver ion diffusion that can be deduced from the simulation done for the highest generator current transient corresponds to a rate of potential change of 380 V/s. However, the initially high rate of the silver ion reduction due to double-layer charging of the sensor undoubtedly and substantially reduces the effective rate of Ag^+ mass transport at the sensor surface. Since our current simulation capabilities do not allow us to explicitly account for the double-layer charging effect in these experiments, we cannot quantitatively assess the effective rate of Ag^+ ion mass transport rate. Nevertheless, the fact that the observed rate of the sensor response increases with each increase in the generator current allows us to hypothesize that the sensor response is mass transport limited. To substantiate this hypothesis, we ask: if we assumed that the sensor response is limited by the kinetics of Ag^+ reduction, what would be the rate constant of electron transfer that could be obtained from the maximum observed rate of sensor potential change (85 ± 5 V/s for the transient recorded at the highest generator current)? We then compare it to literature data. To do this, we first relate the maximum rate of potential change (dE/dt) in Fig. 3 to the instantaneous magnitude of the charging current i and to the sensor's interfacial capacitance C_{dl} (the latter is assumed to be independent of the sensor potential):

$$i = C_{dl}A\frac{dE}{dt} \tag{2}$$

If we now assume that this current is kinetically controlled, we can evaluate it in terms of k_0:

$$i = nFAk_0C\exp\left[-\frac{\alpha nF}{RT}(E - E'^{o})\right] \tag{3}$$

The capacitance of the Ag micro-sensor was measured independently (see below) to be 33 ± 1 μF/cm^2. Using the value of E of 0.180 V at the point of maximum slope, and the corresponding concentration of Ag^+ ions at the sensor surface, we obtain k_0 of 7.5×10^{-3} cm/s. This value is more than an order of magnitude smaller than the literature value of 0.25 cm/s [22]. Therefore we can conclude that the observed maximum rate of potential change is not limited by the interfacial kinetics, and that it is limited by the mass transport of the silver ions, as we originally hypothesized. While we cannot apply even higher generator currents in order to measure the maximum response rate of this kinetically very fast silver sensor, the experiment in Fig. 3 allowed us to determine that the upper limit of our P-ETOF experiment to measure rates of sensor potential change is ~80 V/s. (This limit depends on the magnitude of the diffusion constant of the electro-generated species.) As we see below, the intrinsic rate of potential change of the AEIROF pH micro-sensors does not exceed this limit.

A typical voltammetric signature of an electrochemically-deposited iridium oxide coating on a gold electrode is shown in Fig. 4. The magnitude of the anodic and cathodic currents corresponding to the Ir(IV/III) states scales with the thickness of the deposited material. The position of the peaks shifts with pH (see inset) exhibiting a supernernstian slope of 80 ± 2 mV/decade. These general properties of the AEIROF are consistent with literature reports [5, 6, 24, 25, 29, 32, 34, 35]. The fact that the deposition of this material involves electrochemically-induced precipitation allows us to form pH-sensitive micro-sensors. The subsequent experiments involved measurements of the dynamic properties of these sensors. Two sets of P-ETOF data obtained at different rates of proton generation and for AEIROF of different thickness and are shown in Fig. 5. As in the case of the silver P-ETOF experiments of Fig. 3, all proton *E-t* transients exhibit capacitive delay. The latter become more severe in the case of the thicker AEIROF sensors. Unlike in the silver ion experiments, the stepwise increase of the proton generation rate ultimately results in the *E-t* transients of the same slope. We also point out that the maximum slope values of 34 V/s and 9 V/s for the 40 and 650 nm-thick films, respectively, are substantially lower than the mass transport limit determined in the Ag^+ P-ETOF experiment. Clearly, in this experiment, by increasing the proton mass transport rates we reached a kinetic limitation of the micro-sensor response. Importantly, the maximum slope values depend on the thickness of the deposited AEIROF. When we examined two additional AEIROF micro-sensors with thicknesses of 120 and 400 nm, the four values of the maximum rates of potential change showed a linear decrease with the AEIROF thickness. This evidence

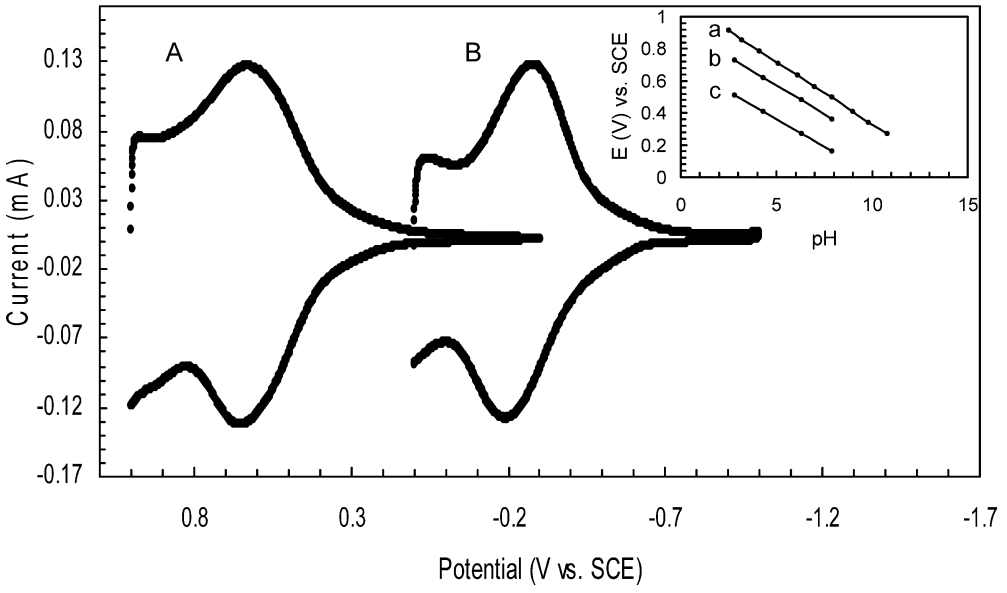

Fig. 4 Cyclic voltammograms of a 120 nm-thick AEIROF deposited on a gold electrode ($A = 0.20$ cm^2) recorded in 0.1 M H_2SO_4 (**A**) and in 0.1 M K_2CO_3 (**B**); $v = 50$ mV/s. The inset shows the calibration plots obtained with **a** 193 nm, **b** 129 nm, and **c** 23 nm AEIROF pH sensors

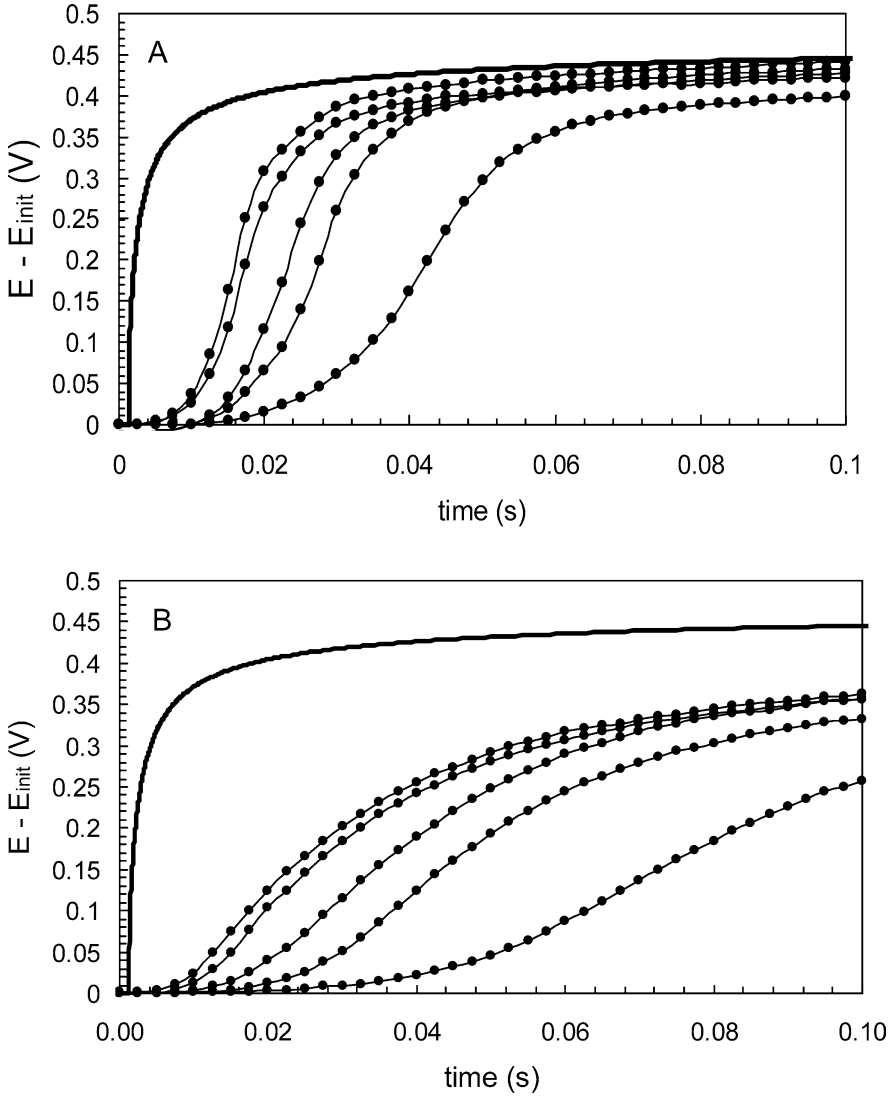

Fig. 5 Two sets of proton P-ETOF(OF) *E-t* transients (connected dots) obtained with the 20 μm gap devices of Fig. 2 with 40 nm-thick (**A**) and 650 nm-thick (**B**) AEIROF micro-sensors. The transients were recorded with a generator current of (left to right) 1, 0.8, 0.5, 0.3, 0.1 mA in a pH 6.8, 1 M $LiClO_4$ solution. In each panel, the heavy continuous line is a numerically simulated transient corresponding to the 1 mA experiment obtained with an independently measured proton diffusion constant of 6.9×10^{-5} cm^2/s

suggests that the pH sensitivity of the iridium oxide films is their bulk property likely to involve proton interaction with the full or a fraction of the volume of AEIROF. We discuss this in more detail below.

Measurements of sensor capacitance

The time delays observed in the P-ETOF experiments discussed in the previous section are due to the finite capacitance of the iridium oxide films. In this section, we present a novel method to measure the capacitances of potentiometric sensors that takes advantage of the capacitive delay phenomenon in our P-ETOF experiments. Our approach required development of "narrow channel" (NC) type ETOF devices described in the "Experimental" section (see Fig. 1). A schematic cross-sectional view of such a device, focusing on the relative positioning of the generator and sensor micro-electrodes is shown in Fig. 6. In view of the fact that the generator-sensor inter-electrode gap (g) of 50 μm is substantially greater than the thickness of the channel of 3.0 μm, diffusion of the electrochemically-generated ions is essentially linear. This allows us to rely on an analytical solution of the diffusion equations to predict the shape of the *E-t* transients [36]. Specifically, the concentration of the generated ions $C(g,t)$ at the sensor (assumed again to be infinitesimally small) is given by the following equation:

$$C(g,t) = C_{\text{init}} + \frac{i}{nFAD}\left\{2\left(\frac{Dt}{\pi}\right)^{1/2}\exp\left(-\frac{g^2}{4Dt}\right) - g\cdot erfc\left[\frac{g}{2(Dt)^{1/2}}\right]\right\} \quad (4)$$

Here C_{init} is the initial, background concentration of the generated ions, and A is the "effective" surface area of the generator electrode taken at the cross-section of the narrow channel, a product of the electrode length l and the channel height h. In other words, the system behaves as if the generator electrode were oriented perpendicular to the long channel of the cell in Fig. 6. The time dependence of the sensor potential can be then obtained assuming its Nernstian response with an experimentally-determined slope value. The agreement between the computed and the recorded *E-t* transients for Ag^+, H^+ as well as Cl^- ions will be the subject of a separate report [37]. Below, we focus on the application of the P-ETOF(NC) methodology to the determination of sensor's capacitance.

Consider first the silver P-ETOF(NC) experiments of Fig. 7. Curve A shows a typical Ag^+ *E-t* transient recorded under moderately high generator current conditions. It is in good agreement with the theoretical calculation using Eq. 4. Such agreement (not involving any adjustable parameters) is observed when neither the initial Ag^+ concentration nor the generator current is very low. As shown in Fig. 7 (curves B and C), significant capacitive delay relative to theoretical expectations is observed when these conditions are not met, and when, as explained above, the demand of the sensor exceeds the supply of the silver ions diffusing from the generator. In order to generate new theoretical *E-t* curves that would correctly predict such transients, we must quantitatively take into account the finite capacitance of the silver micro-sensor. The iterative process involved in generating the theoretical transient (plotted as bold lines in Fig. 7, curves B, C) requires one adjustable parameter – the capacitance of the micro-sensor. The algorithm developed to accomplish this has been described elsewhere [31]. Briefly, the increasing concentration of Ag^+ ions at the sensor is divided into arbitrarily small increments, ΔC, occurring over corresponding small time increments, Δt. We assume that the silver ions contained in the small volume (v) of the solution directly above the micro-sensor ($v = w\times l\times h_1$, see Fig. 6) are in Nernstian equilibrium with the sensor. This requires the iterative computation of the true equilibrium concentration of silver ions and the corresponding sensor potential that takes into account the fact that some of the silver ions (d N) must be reduced to adjust the sensor potential to the true equilibrium value. Clearly, the true equilibrium Ag^+ concentration is smaller than that obtained when only diffusion is considered. Likewise, the true equilibrium potential of the sensor is also smaller and rises less rapidly. As shown above (see Eq. 1), sensor capacitance is the parameter

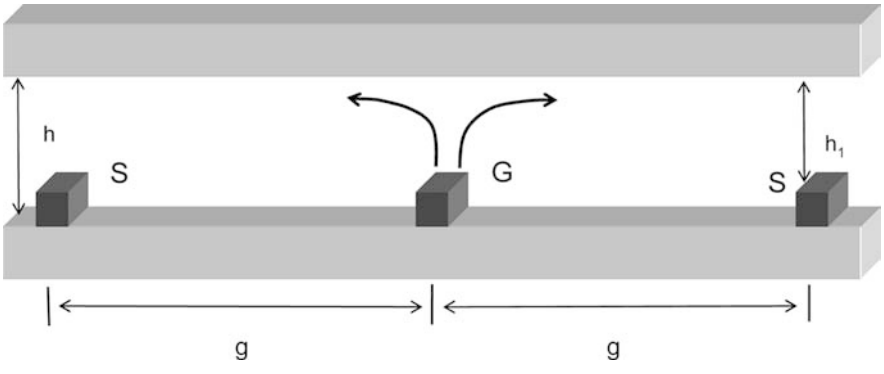

Fig. 6 Cartoon showing a side view of a narrow channel of the P-ETOF device of Fig. 1 (only the central fragment with the generator, G, and the sensor micro-electrodes, S, is shown). The arrows mark the direction of ion diffusion originating at the central generator micro-electrode

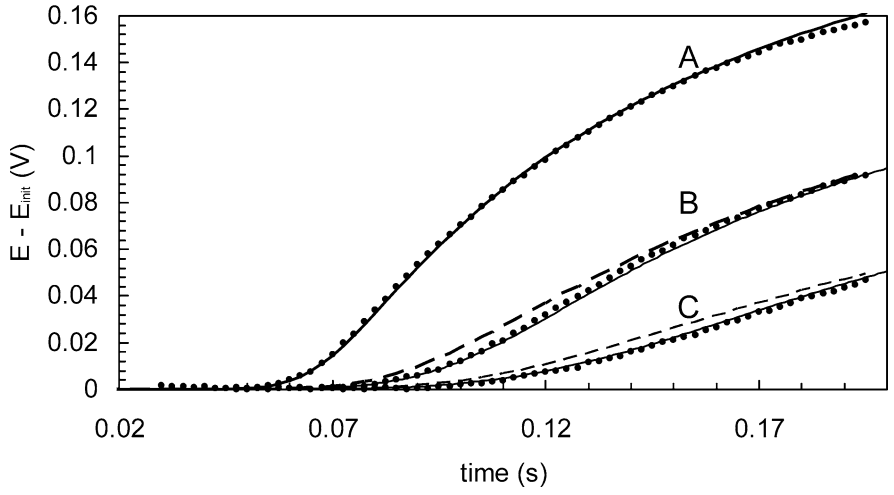

Fig. 7 A set of three experimental Ag^+ P-ETOF(NC) sensor potential versus time transients (closed circles) recorded with the device of Fig. 1 in a 3.5×10^{-5} M $AgNO_3$, 1 M $LiClO_4$ solution at a generator current of 100 μA (**A**), 5 μA (**B**), 1 μA (**C**). The calculated *E-t* transient corresponding to the 100 μA experiment was obtained using Eq. 4. The theoretical transients corresponding to the 5 and 1 μA experiments were obtained using Eq. 4 (dashed lines), and Eq. 4 plus an iterative algorithm incorporating the finite capacitance of the sensor (continuous line)

that determines the magnitude of the silver ion depletion.

Both experimental transients exhibiting capacitive delay in Fig. 7 were adequately fit with a single value of sensor capacitance of 33 ± 1 μF/cm^2, a value that agreed very well with the independent measurements of this sensor's capacitance in the same range of potentials by fast scan voltammetry. While in this case our new P-ETOF method merely duplicates other well-established techniques to measure interfacial capacitance, the benefits of the P-ETOF method can be appreciated when we next examine AEIROF pH micro-sensors.

The proton P-ETOF(NC) experiments were carried out with the same devices as those used in the Ag^+ experiments of Fig. 7. As in those experiments, by selecting a low initial H^+ concentration of 8.5×10^{-5} M, and by using low generator currents (1 and 5 μA), we generated *E-t* transients exhibiting capacitive delays (see Fig. 8). Subsequently, we used the iterative algorithm described above to fit the experimental transients with computed *E-t* curves using a single value of the AEIROF capacitance. The best fitting theoretical transients obtained with C_{dl} of 100 ± 10 μF/cm^2 show a discrepancy at the rising portion of the transients. In other words, the best fit C_{dl} value was selected to optimize the fit at longer times at the expense of the discrepancies at shorter times. The initial discrepancy suggests that the experimental transients are burdened with an additional delay that could be due to kinetics of proton transport within the iridium oxide film. Indeed, the same type of experiments done with AEIROF of different thicknesses in the range of 40–180 nm showed that the apparent capacitances of these sensors increase linearly with the films' thickness with a slope of 3 μF cm^{-2} nm^{-1}. In view of these results, we can report the capacitance of AEIROF to be 30 F/cm^3.

Conclusions

This report is focused on the description of the potentiometric electrochemical time-of-flight methodology and its ability to assess the dynamic properties and the

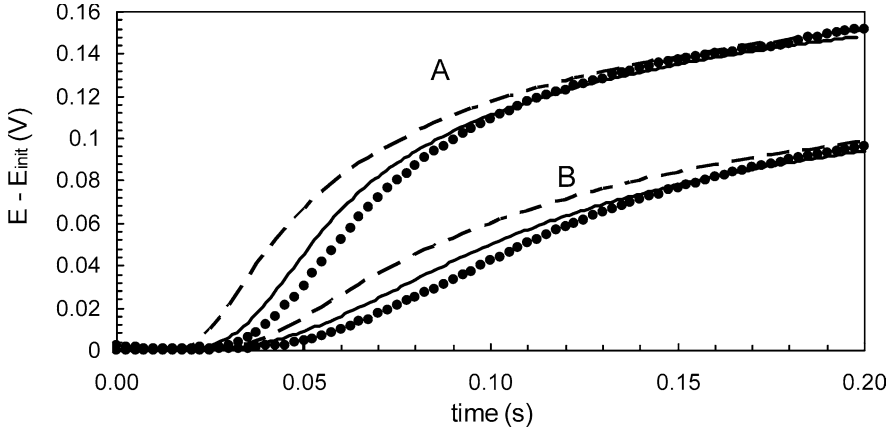

Fig. 8 Two experimental H^+ P-ETOF(NC) sensor potential versus time transients (closed circles) recorded with the device of Fig. 1 in a pH 6.8, 1 M $LiClO_4$ solution at a generator current of 5 μA (**A**) and 1 μA (**B**). The calculated *E-t* transients were obtained using Eq. 4 (dashed lines), and Eq. 4 plus an iterative algorithm incorporating the finite capacitance of the sensor (continuous line)

capacitance of solid-state micro-potentiometric sensors. Using an open face mode of this technique, and high values of the generator current, we demonstrated that rates of sensor potential change as high as ~85 V/s can be measured. In the narrow channel mode, in which electrolyte solution is confined to a 3 μm-thick layer, mass transport of the electro-generated ions between the generator and sensor electrodes obeys linear diffusion equations. While capacitive delays are encountered whenever the initial silver/hydrogen ion concentration and the generator current are low, the exceedingly small volume of a solution directly above a micro-sensor allows us to correct for such delays by explicitly taking into account the capacitance of a sensor micro-electrode. Using these approaches we first characterized silver micro-sensor electrodes. As expected, the kinetics of $Ag^+ + e^- \rightleftharpoons Ag$ are too fast and the largest observed rate of the Ag sensor potential change of 85 V/s is mass transport controlled. The capacitance of a silver microsensor obtained by P-ETOF(NC) of 33 $\mu F/cm^2$ is identical to the values measured by fast scan voltammetry. Subsequent characterization of iridium oxide pH microsensors revealed that both their rate of potential change and the capacitance depend on the thickness of these films reflecting the porous nature of this material. In addition, we observed that the *E-t* transients with a capacitive delay could not be accurately fit with a single value of capacitance. These results strongly suggest that another mechanistic step exists such as slow proton diffusion or migration in the bulk of AEIROF that affects the sensor's response characteristics. The capacitance values reported above for the AEIROF are therefore somewhat approximate. Nevertheless, these preliminary results show that our P-ETOF method offers a tangible measure of sensor capacitance that is otherwise difficult if not impossible to unambiguously obtain by other methods such as impedance spectroscopy [38, 39]. The analytical significance of the capacitance of a potentiometric sensor requires some discussion. This parameter becomes important in cases of potentiometric measurements carried out with microsensors in exceedingly small volumes of analyte solutions [4, 7]. Under such conditions, changes in a sensor's potential, requiring "consumption" of a finite quantity of species of interest, may substantially decrease its concentration and result in a negative error. A priori knowledge of a sensor's capacitance allows one to correct for such errors. It also facilitates optimization of micro-sensor design. The data presented above indicate that AEIROF pH micro-sensors should be designed to minimize the thickness of the iridium oxide film in order to minimize its capacitance.

Acknowledgements We acknowledge the donors of the Petroleum Research Fund, administered by the ACS, for partial support of this research. Additional support was provided by the National Science Foundation (CHE-0079225 and CHE-0416349).

References

1. Lindner E, Buck RP (2000) Anal Chem 72:336A
2. Lauks IR (1998) Acc Chem Res 31:317
3. Mailly SC, Hyland M, Mailley P, McLaughlin JM, McAdams ET (2001) Mat Sci Eng 21:167
4. Spaine TW, Baur JE (2001) Anal Chem 73:930
5. Wipf DO, Ge F, Spaine TW, Baur JE (2000) Anal Chem 72:4921
6. Marzouk SAM, Ufer S, Buck RP, Johnson TA, Dunlap LA, Cascio WE (1998) Anal Chem 70:5054
7. Wei C, Bard AJ, Nagy G, Toth C (1995) Anal Chem 67:1346
8. Slowinska K, Feldberg SW, Majda M (2003) J Electroanal Chem 554–555:61
9. Feldman BJ, Feldberg SW, Murray RW (1987) J Phys Chem 91:6558
10. Licht S, Cammarata V, Wrighton MS (1989) Science 243:1176
11. Cammarata V, Talham D R, Crooks RM, Wrighton MS (1990) J Phys Chem 94:2680
12. Licht S, Cammarata V, Wrighton MS (1990) J Phys Chem 94:6133
13. Tatistcheff HB, Fritsch-Faules I, Wrighton MS (1993) J Phys Chem 97:2732
14. Wittek M, Möller G, Johnson MJ, Majda M (2001) Anal Chem 73:870
15. Rechnitz GA (1964) Talanta 11:1467
16. Johansson G, Norberg K (1968) J Electroanal Chem 18:239
17. Toth K, Gavaller I, Pungor E (1971) Anal Chim Acta 57:131
18. Toth K, Pungor E (1973) Anal Chim Acta 64:417
19. Mertens J, Van den Winkel P, Massart DL (1976) Anal Chem 48:272
20. Yao S, Wang M, Madau M (2001) J Electrochem Soc 148: H29
21. Lindner E, Toth K, Pungor E, Berube TR, Buck RP (1987) Anal Chem 59:2213
22. Gerischer H, Tischer RP (1957) Z Electrochem 61:1159
23. Katsube T, Lauks I, Zemel JN (1982) Sensor Actuator 2:399
24. Yuen MF, Lauks I, Dautremont-Smith WC (1983) Solid State Ionics 11:19
25. Burke LD, Mulcahy JK, Whelan DP (1984) J Electroanal Chem 163:117
26. Fog A, Buck RP (1984) Sensor Actuator 5:137
27. Hitchman ML, Ramanathan S (1988) Analyst 113:35
28. Glab S, Hulanicki A, Edwall G, Ingman F (1989) Crit Rev Anal Chem 21:29
29. Baur J, Spaine TW (1998) J Electroanal Chem 443:208
30. Wang M, Yao S, Madou M (2002) Sensor Actuat B 81:313
31. Slowinska K (2003) PhD dissertation: Micro-electrochemical time-of-flight method with amperometric generation and potentiometric detection. University of California, Berkeley, CA
32. Yamanaka K (1989) Jpn J Appl Phys 28:632
33. Britz D (1988) Digital simulations in electrochemistry, 2nd edn. Springer, Berlin Heidelberg New York
34. Petit M, Plichon V (1998) J Electroanal Chem 444:247
35. Mo Y, Stefan IC, Cai W-B, Dong J, Carey P, Scherson DA (2002) J Phys Chem B 106:3681
36. Galus Z (1994) Fundamentals of electrochemical analysis, 2nd edn. Ellis Horwood/Polish Scientific, New York/Warsaw, Ch 6, Sect 6.1.2.1
37. Elsen HA, Slowinska K, Majda M (2004) unpublished results
38. Aurian-Blajeni B, Beebe X, Rauh RD, Rose TL (1989) Electrochim Acta 34:795
39. Silva TM, Simoes AMP, Ferreira MGS, Walls M, Da Cunha Belo M (1998) J Electroanal Chem 441:5